Draping or overriding: The effect of horizontal stress gradients on internal layer architecture in ice sheets

Richard C. A. Hindmarsh,[1] Gwendolyn J.-M. C. Leysinger Vieli,[2] Mélanie J. Raymond,[3] and G. Hilmar Gudmundsson[1]

Received 29 March 2005; revised 30 October 2005; accepted 26 January 2006; published 16 June 2006.

[1] Internal isochronic layers in ice sheets sensed by radar show two characteristic relationships to the basal topography: Either they override it, with layers above the crests of rises lying essentially flat, or they drape over it, with the layers following rises and falls in basal topography. A mechanical theory is presented which shows that overriding is the expected behavior when topographic wavelengths are comparable with or less than the ice thickness, while draping occurs at longer wavelengths. This is shown with analytical perturbation solutions for Newtonian fluids, numerical perturbation solutions for nonlinear fluids, and finite element solutions for nonlinear fluids and large-amplitude variations. Bed variation from topography and changes in the basal boundary condition are considered, for fixed bed and sliding beds, as well as three-dimensional flows and thermomechanically coupled flows. In all cases, the dominant effect on draping/overriding is the wavelength of the topography or variation in basal boundary conditions. Results of these full mechanical system calculations are compared with those from the shallow ice approximation and the longitudinal stress approximation. Some calculations are carried out for zero accumulation, where the age of the ice and therefore isochrone geometry is not defined. It is shown that there is a close relationship between isochrones and streamlines, and that they behave similarly when bed wavelength divided by the ice thickness is small compared with the ratio of ice velocity and accumulation rate, which is a useful approximation. Numerical comparisons of isochrones and streamlines show them to be virtually coincident.

Citation: Hindmarsh, R. C. A., G. J.-M. C. Leysinger Vieli, M. J. Raymond, and G. H. Gudmundsson (2006), Draping or overriding: The effect of horizontal stress gradients on internal layer architecture in ice sheets, *J. Geophys. Res.*, *111*, F02018, doi:10.1029/2005JF000309.

1. Introduction

[2] Radar-echo sounding of cold ice sheets shows the presence of layers at depth, which are believed to represent former surfaces of the ice sheet. This paper is predicated on the basis that this is true. The layers arise when snowfall events containing material with unusual electric properties, particularly unusual ion concentrations, is deposited on the ice surface [e.g., *Hempel et al.*, 2000]. A typical source for these anomalous materials is volcanic eruptions. Near the surface of the ice sheet, isochronic layers are generally flat, with occasional synclines and anticlines. In general, these near-surface features are believed to be caused by spatial variations in the accumulation rate of snow, with synclines for example being associated with increased accumulation rate. At depth, isochronic layers are much more irregular. Sometimes they drape over and are subparallel to the bed, while at other times they override it, lying almost flat over the most extreme topography. More rarely, they dip toward and outcrop at the bed, showing not only that basal melting has occurred, but that there is spatial variation in the amount of basal melting. This can either be due to variation in the geothermal heat flux or to variations in the frictional heating near or at the base of the ice sheet, attributable to unusual, and therefore interesting, dynamical features.

[3] To exemplify some of these statements, Figure 1 shows an example from near Lake Vostok. The ice flows outward from Ridge B. Three areas are circled: (zone a) a wide depression, (zone b) an area with mountains of constant maximum elevation, and (zone c) an area containing one or two mountains with much greater elevation than their neighbors. It is intuitively obvious that solitary mountains will disturb layers around them. In this paper we are concerned with the contrast between zones a and b in Figure 1. In the former, the lines drape the depression, while in the latter the lines override the depressions. While spatial variation in the accumulation rate is believed to be

[1] British Antarctic Survey, Cambridge, UK.
[2] Bristol Glaciology Centre, School of Geographical Sciences, University of Bristol, Bristol, UK.
[3] Laboratory of Hydraulics, Hydrology and Glaciology, Eidgenossische Technische Hochschule (VAW ETH), Zurich, Switzerland.

0148-0227/06/2005JF000309$09.00

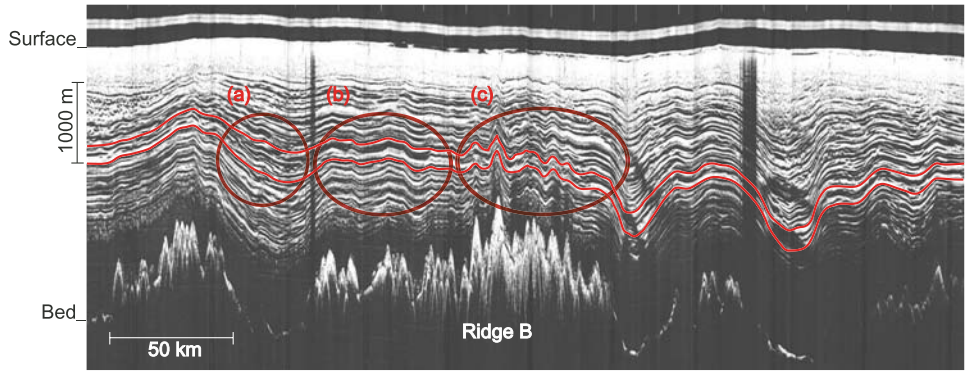

Figure 1. Radargram showing draping over long-wavelength troughs and overriding of short wavelength features. Layers drape over the wide trough (zone a), but override the closely spaced mountains (zone b). Single mountains disturb layers whatever their horizontal dimension (zone c).

the dominant source of undulations in isochronic layers, nearer the bed mechanical effects are expected to play a role at least as significant as that of basal melting. The purpose of this paper is to investigate how mechanical effects affect layer architecture. This paper does not investigate small-scale structures such as folds or thrusts. Surprisingly little work has been done on how glacier mechanics affects isochrone architecture. A classic paper is by *Weertman* [1976], who looks at how changes in the basal boundary from frozen to sliding can lead to dips in isochrones. This can be called the "Weertman effect," and the opposite transition, the "reverse Weertman effect." Another paper is by *Pattyn* [2002], who looks at the effect of topography on isochrone architecture using the longitudinal stress approximation.

[4] Following *Gudmundsson* [2003], one can immediately anticipate that two factors will have a dominating effect: the wavelength of the undulations and the slip ratio (the ratio of the sliding velocity to the difference in velocity between ice surface and bed). These effects are investigated in this paper using flows on infinite sections. The benefit of this configuration is that it isolates other influences, allowing us to focus on the effects of mechanics, but it creates complications with regards to the role the vertical velocity plays in developing isochrones, since this velocity arises to accommodate mass influx at the upper surface and efflux at the lower surface. Fortunately, in the limiting case of no accumulation/no melting, it turns out (and is shown here) that isochrones can be identified with streamlines (in plane flow). This remains a good approximation provided that the product of the ratios of accumulation rate to horizontal velocity and wavelength of bedrock roughness to ice thickness remains small.

[5] We use three different techniques to compute the flow down infinite sections. First, we use the analytical theory developed by *Gudmundsson* [2003], applicable to fluids with a linear rheology, to exemplify the basic effects. This assumes that the amplitude of bed perturbations is "small"; that is, the amplitude of the bed perturbations is a small fraction (<10%) of the ice thickness. Second, we use a semianalytical perturbation theory developed by *Hindmarsh* [2004], which deals with nonlinear rheologies and nonsmall accumulation rates to generalize the examples to more realistic cases. This theory also only treats "small" perturbations in the bedrock. Both perturbation theories can deal with three-dimensional flows. Finally, plane-flow finite element calculations consider nonlinear rheologies where the bedrock perturbation amplitudes are not small. In the formulation of the finite element approach it is assumed that the accumulation rate is zero, but some useful results which show how nonzero accumulation rates affect isochrone architecture can be obtained and can be shown to be decent approximations.

[6] One use of isochronic data is the investigation of the spatial variation of accumulation rate. This remains a large computational problem, acutely so in inverse mode, and the use of vertically integrated approximations such as the shallow ice approximation (SIA) remains essential. In particular, "stream-tube" approximations are useful, where the ice upper and lower surface geometry are given together with the accumulation rate, and mean velocity fields are computed from mass balance, using the SIA and continuity to compute the distribution of horizontal and vertical velocity with depth. This procedure has many attractions; rather than tuning a model to give an approximation to the topography, one automatically uses the correct topography, and comparison of layer architecture with data is considerably facilitated. One factor of crucial importance is how predictions of layer architecture made by the SIA and the full system of balance equations differ. This allows the determination of whether discrepancies between vertically integrated models and data can be attributed to the use of simplified mechanical models. Motivated by this, we present extensive series of results where steady geometries of ice flows are computed using the full system of equations, and isochrone architectures for this particular ice surface geometry are computed for both the full system and for the SIA. While the SIA steady geometry could and often would be different, the comparisons we make are more useful for the reasons outlined above.

[7] The results of all three modes of analysis show that as expected, wavelength is the dominant effect. Isochrones drape around basal topography at long wavelength, while at short wavelength, isochrones override basal topography. In this paper, a long wave has wavelength much greater than the ice thickness, while a short wave has wavelength less than or approximately equal to the ice thickness.

[8] The paper plan is as follows: the governing equations, their scalings and linearizations are presented briefly in

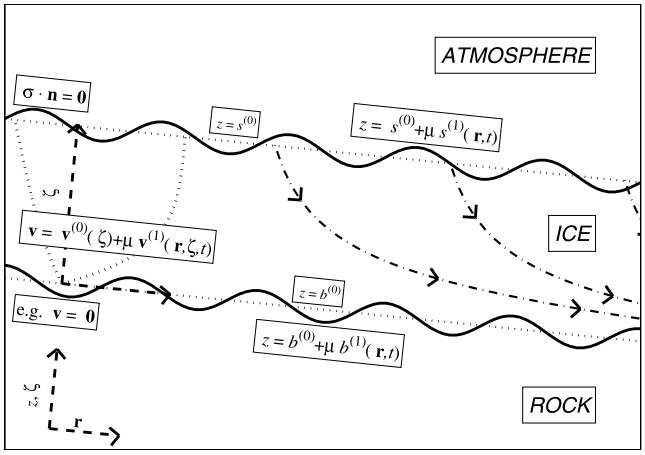

Figure 2. Illustration of the problem set-up and coordinate system.

sections 2 and 3. The relationship between streamlines and isochrones is discussed in section 4. Solutions to the governing equations are presented in section 5, and the results are summarized in the final section. Three appendices present technical details of the formulation and solution of the equations.

2. Stokes Equations

[9] A classic glaciological configuration of flow down the infinite plane is used, and cyclic (repeated) boundary conditions are applied to force variation at the desired wavelength, either by variations in the bed topography or the basal slipperiness. The setup of flow down an infinite plane is illustrated in Figure 2. Dimensional quantities are represented by a tilde and nondimensional quantities without a tilde. Fourier transforms are represented by a caret. The coordinates are $(\tilde{x}, \tilde{y}, \tilde{z})$, where $\tilde{z}$ is perpendicular to the base plane and $\tilde{x}$ is in the zeroth-order flow direction. The $\tilde{z}$ direction is called "vertical" and the $\tilde{\boldsymbol{r}} = (\tilde{x}, \tilde{y})$ plane "horizontal". The upper and lower surfaces are given by $\tilde{z} = \tilde{s}(\tilde{\boldsymbol{r}}, \tilde{t})$, $\tilde{z} = \tilde{b}(\tilde{\boldsymbol{r}}, \tilde{t})$ respectively, the thickness of the ice is given by $\tilde{H}(\tilde{\boldsymbol{r}}, \tilde{t}) = \tilde{s}(\tilde{\boldsymbol{r}}, \tilde{t}) - \tilde{b}(\tilde{\boldsymbol{r}}, \tilde{t})$ and $\tilde{T}$ represents time. Subscripts (s), (b) indicate evaluation at the surface or base, respectively. The operators $\boldsymbol{\nabla}_{\mathrm{H}}$, $\boldsymbol{\nabla}_{\mathrm{H}}\cdot$, represent the horizontal gradient and divergence, respectively.

[10] The three-dimensional velocity field is conveniently represented by the vertical velocity $\tilde{w}$ and the horizontal velocity vector $\tilde{\boldsymbol{u}} = (\tilde{u}_x, \tilde{u}_y)$, and we also use $\tilde{\boldsymbol{v}} = (\tilde{u}_x, \tilde{u}_y, \tilde{w})$. The governing equations, which apply to all $\tilde{\boldsymbol{r}}$ are

$$\boldsymbol{\nabla}_{\mathrm{H}} \cdot \tilde{\boldsymbol{u}} + \partial_{\tilde{z}} \tilde{w} = 0 \qquad \tilde{b} \le \tilde{z} \le \tilde{s}, \tag{1}$$

$$\boldsymbol{\nabla} \cdot \tilde{\boldsymbol{\sigma}} + \tilde{\rho}\tilde{\boldsymbol{g}} = 0 \qquad \tilde{b} \le \tilde{z} \le \tilde{s}, \tag{2}$$

$$\tilde{\boldsymbol{\sigma}}_{(s)} \cdot \boldsymbol{n}_{(s)} = 0 \qquad \tilde{z} = \tilde{s}, \tag{3}$$

$$\left.\begin{aligned} \boldsymbol{v}_{(b)} &= 0, \quad \text{no slip} \\ (\text{see equation (6)})\boldsymbol{n}_{(b)} \cdot \boldsymbol{v}_{(b)} &= \tilde{m}, \quad \text{sliding} \end{aligned}\right\} \qquad \tilde{z} = \tilde{b}, \tag{4}$$

Here (1) expresses conservation of mass in the ice; (2) describes conservation of momentum in the ice, and (3) and (4) are momentum equation boundary conditions, where $\tilde{\boldsymbol{\sigma}}$ is the stress tensor, $\tilde{\rho}$ is the density of ice, $\tilde{\boldsymbol{g}} = \tilde{g}(\varepsilon, 0, -1)$ is the gravitational acceleration vector and $\boldsymbol{n}$ is the outward normal vector at the indicated surface. The horizontal component of gravity $\varepsilon\tilde{g}$ is functionally equivalent to a slope of ε. The constitutive relations comprise (1) a nonlinear viscous relationship within the ice,

$$\tilde{\mathsf{e}} = \tilde{A}_c |\tilde{\tau}|^{n-1} \tilde{\tau}, \tag{5}$$

where $\tilde{\mathsf{e}}$ is the strain rate tensor, $\tilde{\tau}$ is a second invariant of the deviator stress tensor $\tilde{\boldsymbol{\tau}}$, n is the Glen index and $\tilde{A}_c$ is a rate factor; and (2) an isotropic sliding relation of the form

$$\tilde{\boldsymbol{u}}_{\|(b)} = \tilde{A}_s \left|\tilde{\boldsymbol{T}}_{t(b)}\right|^{\ell-1} \tilde{\boldsymbol{T}}_{t(b)} / \tilde{p}_e^{\nu}, \tag{6}$$

where $\tilde{\boldsymbol{u}}_{\|(b)}$ is the sliding velocity, $\tilde{\boldsymbol{T}}_{t(b)}$ is the basal tangential traction, ℓ is the sliding index, $\tilde{A}_s$ is the sliding rate factor, $\tilde{p}_e = -\tilde{T}_n - \tilde{p}_w$ is the effective pressure, $\tilde{T}_n$ is the normal traction, $\tilde{p}_w$ is the subglacial water pressure and ν is a further index.

[11] The heat equations are given by

$$\partial_{\tilde{t}}\tilde{\theta} + \tilde{\boldsymbol{v}} \cdot \nabla\tilde{\theta} = \tilde{\kappa}\boldsymbol{\nabla}^2\tilde{\theta} + \frac{\tilde{D}}{\tilde{\rho}\tilde{c}} \qquad \tilde{b}(\tilde{\mathbf{r}}, \tilde{t}) \le \tilde{z} \le \tilde{s}(\tilde{\mathbf{r}}, \tilde{t}), \tag{7}$$

$$\tilde{\theta}_{(s)} - \tilde{\theta}^s = 0 \qquad \tilde{z} = \tilde{s}(\tilde{\mathbf{r}}, \tilde{t}), \tag{8}$$

$$\tilde{K}_i \boldsymbol{\nabla}\tilde{\theta}_{(b)} \cdot \mathbf{n}_{(b)} = -\tilde{Q}_G \qquad \tilde{z} = \tilde{b}(\tilde{\mathbf{r}}, \tilde{t}). \tag{9}$$

Equations (7)–(9) represent conservation of heat in the ice, where $\tilde{\theta}$ is the temperature in the ice, $\tilde{\theta}^s$ is the prescribed surface temperature, $\tilde{\kappa}$ is the thermal diffusivity of ice, $\tilde{c}$ is the specific heat capacity, $\tilde{D} = \frac{1}{2}trace(\tilde{\tau} \cdot \tilde{\mathbf{e}})$ is the dissipation, $\tilde{\boldsymbol{\tau}}$ is the deviatoric stress and $\tilde{K}_i$ is the thermal conductivity of ice and $\tilde{Q}_G$ is the geothermal heat flux. When modeling the flow of heat, only cases where the bed is below melting point (i.e., no sliding) are considered.

[12] The assumption of quasiuniform flow states that such a flow $\tilde{\boldsymbol{v}}^{(\mathrm{QU})}$, where superscript (QU) indicates a quasiuniform flow, is given by

$$\tilde{\boldsymbol{v}}^{(\mathrm{QU})} = \left(\tilde{v}_{\tilde{x}}^{(\mathrm{QU})}, 0, \tilde{v}_{\tilde{z}}^{(\mathrm{QU})}\right) \qquad \boldsymbol{\nabla} \cdot \tilde{\boldsymbol{v}}^{(\mathrm{QU})} = 0,$$

where $\tilde{\boldsymbol{v}}^{(\mathrm{QU})}$ is treated as being independent of $\tilde{\boldsymbol{r}}$, but $\partial_{\tilde{x}}\tilde{v}_{\tilde{x}}^{(\mathrm{QU})}$ may be nonzero. Essentially, it is being assumed that over one wavelength $\partial_{\tilde{x}}\tilde{v}_{\tilde{x}}^{(\mathrm{QU})}$ is sufficiently small that the $\tilde{\boldsymbol{r}}$ independence of $\tilde{\boldsymbol{v}}^{(\mathrm{QU})}$ is a valid assumption. This assumption is applied to the base flow about which linearization is performed.

[13] The upper and lower surface kinematical conditions are

$$\left.\begin{aligned} \partial_{\tilde{t}}\tilde{s} + \tilde{\boldsymbol{u}}_{(s)} \cdot \boldsymbol{\nabla}\tilde{s} &= \tilde{w}_{(s)} + \tilde{a}, \\ \tilde{\boldsymbol{u}}_{(b)} \cdot \boldsymbol{\nabla}\tilde{b} &= \tilde{w}_{(b)} + \tilde{m}, \end{aligned}\right\}, \tag{10}$$

where a, m are the surface accumulation and basal melting respectively. The age equation is simply the advection equation for the age $\tilde{X}$ with a source term,

$$\partial_{\tilde{t}}\tilde{X} + \tilde{\boldsymbol{v}} \cdot \boldsymbol{\nabla}\tilde{X} = 1, \tag{11}$$

with boundary conditions

$$\tilde{X} = 0, \tilde{\boldsymbol{v}} \cdot n_{(b)} < 0. \tag{12}$$

3. Scaling, Mapping, Linearizations, and Solution Methods

3.1. Scaling

[14] The main function of dimensional analysis as used in this paper is to reduce the number of free parameters. In the related analysis of *Raymond and Gudmundsson* [2005], there are two free parameters, the slip ratio and the mean slope ε. In some cases here, we also consider nonzero accumulation, which is a third free parameter. Other parameters (e.g., ice thickness) are shown by the dimensional analysis not to be truly independent parameters. The results of *Raymond and Gudmundsson* [2005] suggest that slope is less important than slip ratio, and for reasons of space slope and accumulation rate are not investigated systematically.

[15] This paper deals with many distinct but closely related quantities, and the notation follows a fairly strict system. A superscript with parentheses containing 0 or 1 refers to the perturbation order in the linearization parameter μ introduced below in (14). Superscripts without parentheses always occur at the rightmost end of the superscript chain, and are exponents. Subscripts without parentheses occur at the leftmost end of the subscript chain. These can refer to tensor or vector components, or to other quantities, which will be clear from the context. Parenthetic subscripts are either (s) or (b), and refer to evaluation of the quantity at the surface and base, respectively. Note that the subscripts without parentheses on A refer to deformation model and not position of evaluation. For example, $\tau^{(1)2}_{xz(b)}$ is the dimensionless first-order horizontal plane shear stress in the x-direction, raised to the power 2, evaluated at the base.

[16] The variables are nondimensionalized as follows. Thicknesses H, elevations z, s, b and horizontal positions $\boldsymbol{r} = (x, y)$ are scaled by $\tilde{H}_*$, (asterisk subscripts imply a scale magnitude). Dimensionless field quantities within the ice are expressed in a normalized vertical coordinate ζ defined by

$$0 \le \zeta = \tilde{H}^{-1}\left(\tilde{z} - \tilde{b}\right) = H^{-1}(z - b) \le 1. \tag{13}$$

Hindmarsh and Hutter [1988] and *Hindmarsh* [1999] write out the associated differential transforms. In physical units the operators $\nabla_{\mathrm{H}}\cdot, \nabla_{\mathrm{H}}$ act in the $(\tilde{\boldsymbol{r}}, \tilde{z})$ coordinate system, while in the dimensionless system they act in the $(\boldsymbol{r}, \zeta)$ system. Pressure and stresses are scaled by $\varepsilon\tilde{\rho}\tilde{g}\tilde{H}_*$, where $\tilde{g} = |\tilde{\boldsymbol{g}}|$ is the acceleration due to gravity. In dimensionless form, the gravity vector $\boldsymbol{g}$ has components $(\varepsilon, 0, -1)$ where $\varepsilon^2 \ll 1$. The velocity scale $\tilde{v}_*$ is chosen so as to set the horizontal velocity u_x for the rheologically equivalent but uniform-bedded cases equal to unity. Specifically, for the linearization studies, this means that $u^{(0)}_{x(s)} = 1$. The accumulation rate a, melting rate m and the velocity $\boldsymbol{v}$ are scaled by $\tilde{v}_*$, the flux has scale given by $\tilde{q}_* = \tilde{v}_* \tilde{H}_*$ and time is scaled by $\tilde{t}_* = \tilde{H}_* / \tilde{v}_*$. These scalings imply $\tilde{A}^*_c = \tilde{v}_*/(\tilde{H}_* \tilde{\tau}^{*n})$, $\tilde{A}^*_s = \tilde{v}_*/\tilde{\tau}^{*(\ell-\nu)}$.

3.2. Linearization for Small-Amplitude Perturbations

[17] We employ linearization techniques to increase the range of situations that can be investigated: in this study, three dimensional flows and thermomechanical coupling. These studies involve far less computational effort than the finite element computations discussed below. The linearizations do assume "small" topography, i.e., topographic amplitudes less than 10% of the ice thickness, which is an ideal that is fairly frequently achieved under ice sheets. Finite (i.e., with no restriction to smallness) amplitudes are considered in the next section.

[18] Linearizations involve a basic flow about which small perturbations are permitted. In this case, the basic flow is a uniform shearing flow along the infinite plane. As well as internal shearing, sliding over the bed is permitted. Furthermore, we consider the flow of heat within the ice, warmed at the bed by geothermal heating and moving through the ice by advection and conduction. Even though the flow is uniform, this assumption can be relaxed slightly to include quasiuniform flows, whereby a nonzero accumulation rate is considered, on the understanding that it is sufficiently small not to increase flow speeds over one wavelength. This accumulation rate advects both cold and tracers (e.g., age markers) downward.

[19] Specifically, in certain of the results discussed below, the relevant field variables are subsequently linearized with a small parameter μ about a base case solution (steady uniform flow down the infinite plane), for example,

$$H = H^{(0)} + \mu H^{(1)}(\mathbf{r}, t) \qquad v = v^{(0)} + \mu v^{(1)}(\mathbf{r}, \zeta, t), \tag{14}$$

etc. These are used to derive a set of zeroth- and first-order equations expressing conservation of mass and momentum. A Fourier transform in the horizontal plane is then applied to the first-order equations, and the first-order fields can be expressed as plane waves,

$$\left.\begin{aligned} H^{(1)} &= \Re\left\{\hat{H}^{(1)} \exp(\lambda t - \mathrm{i}\boldsymbol{k} \cdot \boldsymbol{r})\right\} \\ \boldsymbol{v}^{(1)} &= \Re\left\{\hat{\boldsymbol{v}}^{(1)}(\zeta) \exp(\lambda t - \mathrm{i}\boldsymbol{k} \cdot \boldsymbol{r})\right\} \end{aligned}\right\}, \tag{15}$$

etc., where $\Re$ represents the real part. In particular, $\hat{H}^{(1)} = \hat{s}^{(1)} - \hat{b}^{(1)}$. In (15), λ is the eigenvalue, the wave numbers are given by $\boldsymbol{k} = (k_x, k_y)$ and the caret indicates the Fourier coefficient of the transform over the $\boldsymbol{r}$-plane only. The scaling is constructed to ensure that $H^{(0)}$ and as many more as possible of the other zeroth-order quantities are unity. Details are given by *Hindmarsh* [2004]. In addition, the case of a Newtonian rheology is also considered, where analytical solutions exist [*Gudmundsson*, 2003].

3.3. Finite Element Solution for Finite Amplitude Perturbations

[20] In addition, finite element solutions of the full Stokes equations in plane flow are computed using the MARC software package [*Leysinger Vieli and Gudmundsson*, 2004; *Raymond and Gudmundsson*, 2005]. These permit nonsmall variations in the basal properties, which is particularly necessary for the variations in basal slipperiness considered

here. These are computed for repeated flow sections with cyclic boundary conditions. No accumulation or basal melting were specified, implying that the assumption of quasiuniform flow is not needed. This leads to difficulties with the usual Glen rheology at small amplitudes, as the ice becomes very viscous near the upper, traction-free, surface owing to the low stresses and strain rates. These difficulties are discussed by *Raymond and Gudmundsson* [2005], but we only consider large amplitudes, where strain rates at the surface are large, and these difficulties do not need to be considered. We report results for steady state flows only.

4. Relationship Between Isochrones and Streamlines

[21] Where there is no recharge (accumulation or basal melting), there is no meaningful solution to the age equation. In particular, to interpret the finite element solutions, it is necessary to consider the relationship between isochrones and streamlines, which are easily computed. In this section the relationship between the two is examined and it is shown that streamline geometry gives useful information about isochrone geometry in plane flow. Streamlines are flow trajectories. In general, they are not coincident with isochrones. Intuitively, one would expect them to be related, and we show here that in plane flow, under certain auxiliary conditions, isochrones and flow lines track each other. For example, over short distances, if a streamline dips, the isochrone dips in a similar way.

[22] More specifically, the two lines are approximately coincident in a particular sense, and it is shown below that the horizontal gradient of age following a streamline is smaller than horizontal gradients of age following other lines (apart from the isochrones), for example, the elevation z or the normalized elevation ζ. This is the strongest statement that can be made; if streamlines and isochrones were coincident, this horizontal gradient would be zero. In cases where there is no accumulation rate, one result of this section is that the streamlines are the limiting isochrone geometry for very small accumulation rates.

[23] To show this, it is convenient to write the partial flux q in terms of the overall flux using a shape function [e.g., *Reeh and Paterson*, 1988], $\omega(x, \zeta)$

$$\left.\begin{array}{rcl} q_x(x,\zeta) & = & \omega(x,\zeta)Q_x(x) \\ \omega(x,0) & \equiv & 0 \\ \omega(x,1) & \equiv & 1 \end{array}\right\}. \tag{16}$$

The steady state age equation in ζ-coordinates can then be written

$$\frac{\zeta\partial_x Q_x - \partial_x(\omega Q_x) - \zeta(a-m) - m}{H}\partial_\zeta X + \frac{Q_x}{H}\upsilon\partial_x X = 1. \tag{17}$$

For the next demonstration it is convenient to use the shape factor as the coordinate system. A further coordinate system using $\breve{\omega} = \omega(x, \zeta)$ as the vertical coordinate can then be defined,

$$\left.\begin{array}{l} X_\omega(x_\omega,\breve{\omega}) = X(x,\zeta) \\ x_\omega = x,\ \breve{\omega} = \omega(x,\zeta) \end{array}\right\}. \tag{18}$$

Mathematically, $\breve{\omega}$ is an independent variable while ω is a dependent variable, but numerically they are equal. We are simply using a new vertical coordinate as it allows us to explore the relationship between streamlines and isochrones. This coordinate system is not used in numerical calculations. This assumes that ω increases monotonically with ζ, which is equivalent to assuming that there are no reverse (circulatory) flows. Differential equations can be transformed in $(x_\omega, \breve{\omega})$-coordinates, using the following differential transforms:

$$\begin{bmatrix} \dfrac{\partial X}{\partial x} \\ \dfrac{\partial X}{\partial \zeta} \end{bmatrix} = \begin{bmatrix} 1 & \dfrac{\partial \omega}{\partial x} \\ 0 & \dfrac{\partial \omega}{\partial \zeta} \end{bmatrix} \begin{bmatrix} \dfrac{\partial X_\omega}{\partial x_\omega} \\ \dfrac{\partial X_\omega}{\partial \breve{\omega}} \end{bmatrix}. \tag{19}$$

There is an important distinction between $\dfrac{\partial X}{\partial x}$, which is the horizontal gradient of the age X on a line of constant ζ (normalized elevation) and $\dfrac{\partial X}{\partial x_\omega}$, which is the horizontal gradient of the age X on a line of constant ω. Substitution of (18) and (19) into (17) gives

$$\breve{\upsilon}\frac{\zeta\partial_x Q_x - \breve{\omega}\partial_x Q_x - Q_x\partial_x\omega - \zeta(a-m) - m}{H}\partial_{\breve{\omega}} X_\omega + \frac{Q_x}{H}\breve{\upsilon}(\partial_{x_\omega} X_\omega + \partial_x\omega\partial_{\breve{\omega}} X_\omega) = 1, \tag{20}$$

where

$$\breve{\upsilon}(x,\breve{\omega}) = \upsilon(x,\zeta) = \frac{\partial\omega(x,\zeta)}{\partial\zeta}.$$

Equation (20) simplifies immediately to

$$\frac{Q_x}{H}\breve{\upsilon}\partial_{x_\omega} X_\omega + \breve{\upsilon}\frac{\zeta\partial_x Q_x - \breve{\omega}\partial_x Q_x - \zeta(a-m) - m}{H}\partial_{\breve{\omega}} X_\omega = 1,$$

and then to

$$\frac{Q_x}{H}\partial_{x_\omega} X_\omega - \frac{\breve{\omega}(a-m) + m}{H}\partial_\omega X_\omega = \frac{1}{\breve{\upsilon}}, \tag{21}$$

which is the steady state age equation in $(x_\omega, \breve{\omega})$-coordinates.

[24] Since ice is entering from the top of the glacier, both terms on the left-hand side must contribute to the balance, while the right-hand side is $\mathcal{O}(1)$ by construction. This implies that $\partial_\omega X_\omega = \mathcal{O}(1/a)$. (For simplicity, we ignore the boundary layer at the bottom where $\breve{\upsilon} = \mathcal{O}(a)$, $\partial_\omega X_\omega = \mathcal{O}(1/a^2)$; the existence of this layer does not affect the following argument.)

[25] Compare (21) with the same equation in ζ-coordinates,

$$\frac{Q_x}{H}\partial_x X - \frac{\omega(a-m) + \partial_x\omega Q_x + m}{H}\partial_\zeta X = \frac{1}{\upsilon}.$$

Again, $\partial_\zeta X = \mathcal{O}(1/a)$. Furthermore, over short range L_x, the term $\partial_x\omega$ will be order $\mathcal{O}(1/L_x)$, and if $L_x < 1/a$

$$\frac{Q_x}{H}\partial_x X - \frac{\partial_x\omega Q_x}{H}\partial_\zeta X \approx 0,$$

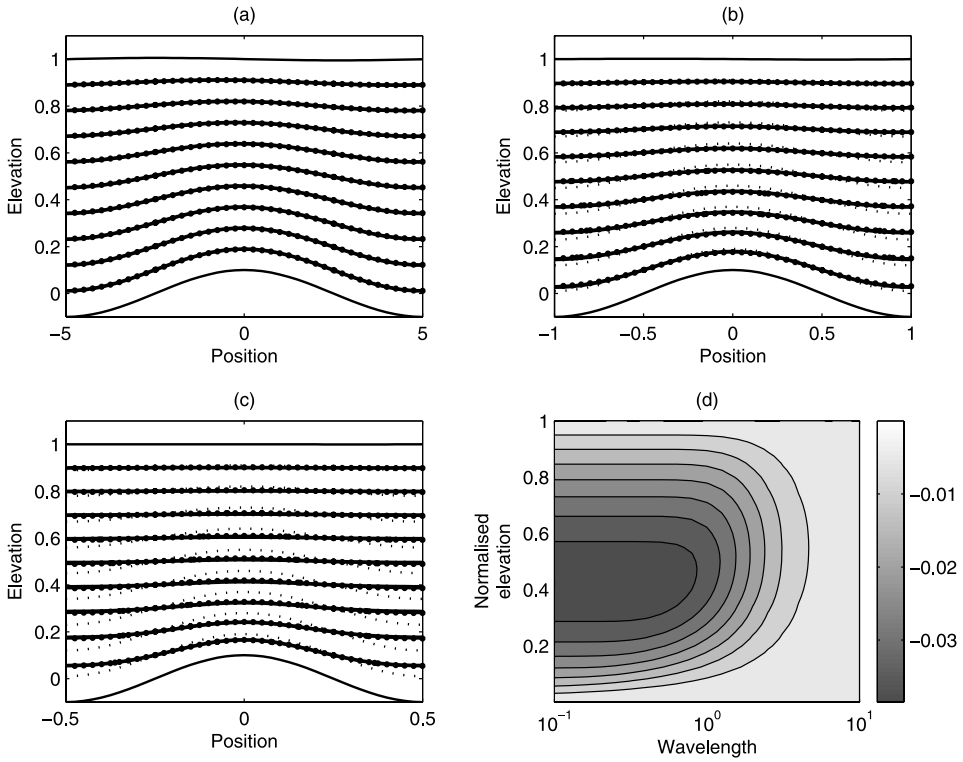

Figure 3. Comparison of streamlines from full system (solid line), longitudinal stress approximation (small circles) and SIA (dotted line), from analytical solutions for Newtonian rheology. The longitudinal stress approximation isochrones almost overlie the full system. All cases are for a bed perturbation amplitude of 0.1. Streamlines closely correspond to isochrones (see Figure 9). (a, c) Comparisons for the indicated wavelength. (d) Isochrone deflection, normalized by ice thickness of the full-system isochrones from the SIA isochrones as a function of elevation and wavelength.

implying both terms on the left-hand side are $\mathcal{O}\left(\frac{1}{aL_x}\right)$ and in particular that

$$\partial_x X = \mathcal{O}\left(\frac{1}{aL_x}\right).$$

However, in $(x_\omega, \breve{\omega})$-coordinates, there are no terms in the age equation (21) of $\mathcal{O}\left(\frac{1}{aL_x}\right)$. The vertical advection term and the source term are $\mathcal{O}(1)$. The horizontal advection term can be safely written as

$$\partial_{x_\omega} X = \mathcal{O}(1), \tag{22}$$

showing that it is much smoother than $\partial_x X$.

[26] Finally, we must deal with the fact that lines of constant ω are not exactly streamlines, even in steady flow. These are given by contours of q_x. It can be readily seen that $\partial_x Q_x = \mathcal{O}(a)$ and that

$$\partial_x q_x = \omega \partial_x Q_x + Q \partial_x \omega = \omega \mathcal{O}(a) + \mathcal{O}(1/L_x), \tag{23}$$

meaning that for length scales $L_x < 1/a$ variations in ω with horizontal position make the lead order contribution to the horizontal gradient of the partial flux q_x and thus to streamline variation. Lines of constant ω therefore correspond to streamlines over these short length scales.

[27] The equivalence of lines of constant ω with streamlines over short distances (equation (23)) and the fact that the horizontal gradient of the age is very much smaller when considered along lines of constant ω are the basis of the statement that isochrones track streamlines over distances shorter than $1/a$. This distance is measured in ice sheet thicknesses. If a is 0.01 (i.e., the accumulation is one hundredth of the ice velocity), then the distance is 100 ice sheet thicknesses. Another way of looking at this is to say that streamlines are the limiting geometry of isochrones as the accumulation rate tends to zero.

[28] A further useful observation is that a feature of the isothermal shallow ice approximation is that $\omega(\zeta)$ is a uniform function. Thus, for the isothermal SIA with constant slip ratio, the property of tracking a streamline also implies tracking a constant normalized elevation. This happens over wavelengths that are $\lesssim \mathcal{O}(1/a)$, but are still sufficiently long that the SIA remains valid.

5. Solutions

5.1. Analytical Perturbation Solutions for Newtonian Rheology

[29] Our first question is whether we can relate simply isochrone geometry to wavelength. A feature common to all three types of analysis is comparing the results to those obtained with the SIA, which is the mechanical approximation most commonly used in large-scale ice sheet modeling,

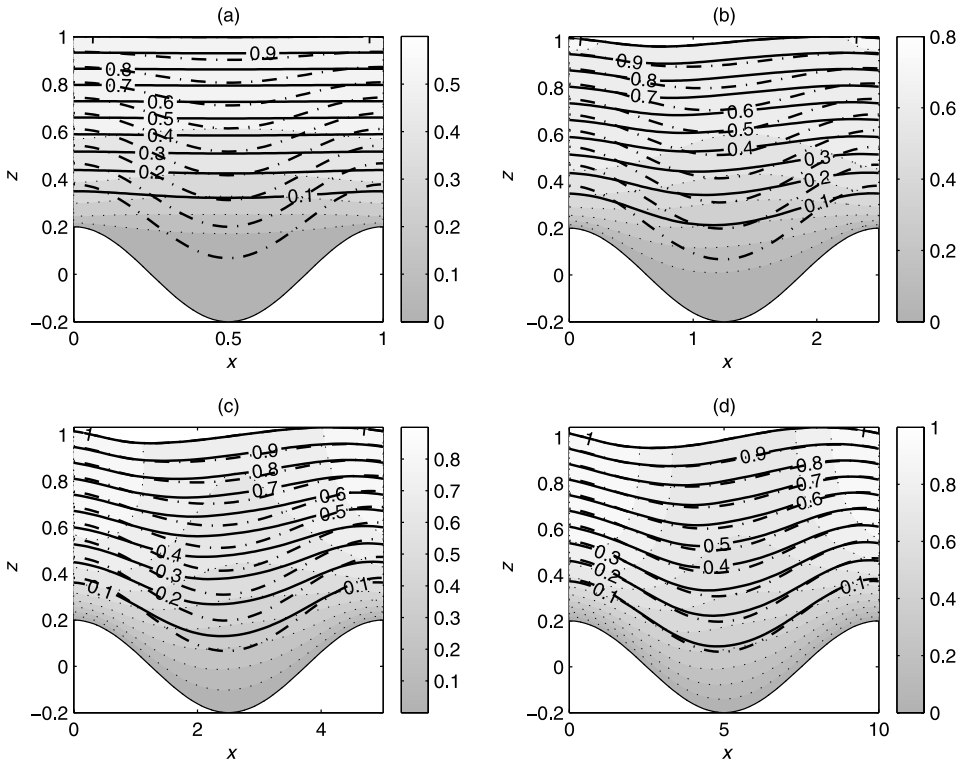

Figure 4. Calculation showing effect of bed perturbations on full system finite amplitude calculations of streamlines/isochrones. Ice is fixed to the bed. Solid lines are full-system (FS) isochrones, dash-dotted lines are shallow-ice approximation (SIA) isochrones, and dotted lines and shading are contours of horizontal velocity. Bed perturbation amplitude is 0.2. Four plots are for indicated wavelengths, in units of ice thickness. Overriding of FS isochrones occurs for short wavelengths; draping occurs at long wavelengths. SIA isochrones always show draping.

especially of isochrones and other tracers. Note from the immediately preceding discussion that this involves looking at the deflection from a constant normalized elevation in cases where the material properties of the ice and bed are uniform. Here we consider a simple Newtonian material. and look at isochrone deflection from the SIA.

[30] The analytic perturbation solution of *Gudmundsson* [2003] (full system) and *Hindmarsh* [2004] (longitudinal stress approximation) can be used to demonstrate the basic effects of wavelength on streamline geometry and thus on isochrone architecture. The solutions have a free surface which responds to perturbations in the basal topography and, where sliding is occurring, in the slipperiness. The solutions apply to a linear rheology with zero accumulation and melting.

[31] The shallow ice approximation predicts velocity shape functions to be independent of wavelength, meaning that flow lines are maintained at the same normalized coordinate provided the rate factor distribution does not change with horizontal position. To order $\mathcal{O}(aL_x)$ this is also true for isochrones. A more mathematical discussion of shape functions and how they are used is given in Appendix C.

[32] Figure 3 demonstrates the effects of non-SIA stresses on isochrone elevation by using the *Gudmundsson* [2003] solution in equation (A14). Also shown are isochrones computed using the longitudinal stress approximation (LSA) of *Blatter* [1995], using the analytical solution for a Newtonian rheology [*Hindmarsh*, 2004, Appendix C], as well as SIA isochrones. As explained above, the full-system (FS) geometry is used for all cases; this only introduces a small error as the transfer of basal topography to surface topography is very similar for all the cases. The figure clearly shows that at relatively short wavelengths, FS isochrones override while SIA isochrones drape, but at long wavelengths, as expected, the SIA and FS isochrones are coincident. More surprising is the degree to which the LSA approximation isochrones are virtually coincident with the FS isochrones over a broad range of wavelengths.

5.2. Numerical Solutions for Finite Amplitude Perturbations

[33] Having obtained some rather straightforward results for a Newtonian fluid, our next question is to ask whether they hold for a material with a more complicated rheology. In partial answer, we introduce a Glen (power law) rheology, sliding at the bed with, in certain cases, spatial variation in the bed slipperiness.

[34] Details of these finite element calculations are given in Appendix B. Since there is no surface mass exchange, ages and therefore isochrones are not meaningfully defined. However, as shown in section 4 and Figure 9 in section 5.3.1, streamlines and isochrones are virtually coincident over short wavelengths. Thus we present results for streamlines in this section, but they also apply to isochrones. Cyclic boundary conditions are applied at the upstream and downstream ends.

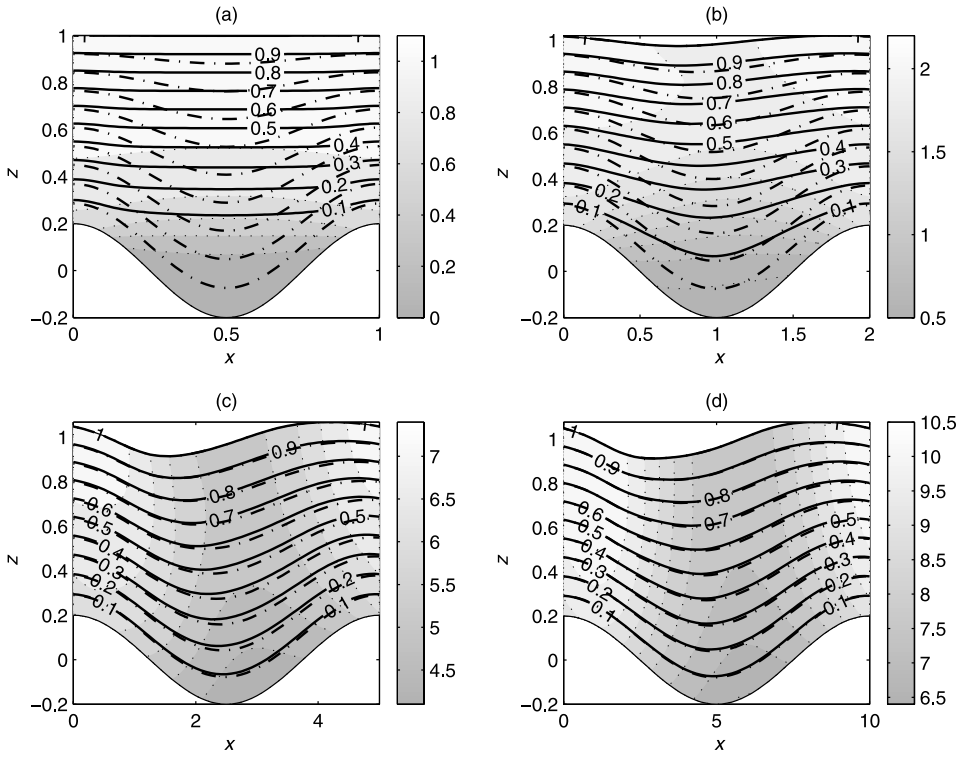

Figure 5. Calculation showing effect of bed perturbations on full system finite amplitude calculations of streamlines/isochrones. Ice is sliding over bed with mean slip ratio C_o of 10. See Figure 4 caption for meaning of different lines. Overriding of FS isochrones occurs for short wavelengths; draping occurs at long wavelengths. SIA isochrones always show draping.

5.2.1. Perturbation to Basal Topography, No Sliding

[35] In these calculations we repeat the perturbation analysis carried out for a linear rheology, using a nonlinear rheology. Figure 4 shows FS and SIA streamlines for flows with fixed beds, at different wavelengths. The bed topography is undulating. The FS solution shows overriding at short wavelengths and draping at long wavelengths. The horizontal velocity contouring shows that the flow stagnates in hollows at short wavelengths, which leads to the overriding.

5.2.2. Perturbation to Basal Topography, Constant Sliding

[36] We now consider the effect of sliding on layer geometry. Figure 5 shows FS and SIA streamlines for flows with sliding at the beds with constant mean slip ratio $C_o = 10$, at different wavelengths. The bed topography is undulating. As with the fixed bed, the FS solution shows overriding at short wavelengths and draping at long wavelengths.

5.2.3. Flat Bed, Sinusoidal Slipperiness Variation

[37] A further means of basal forcing is horizontal variation in the basal slipperiness, which affects the vertical distribution of flux. Figure 6 shows FS and SIA streamlines for flows with sliding at the beds with sinusoidally varying slipperiness and mean slip ratio $C_o = 10$, amplitude 0.2. In this case the FS and SIA streamlines are virtually coincident. At long wavelength there is a marked surface response, and the upper streamlines track the upper surface.

5.2.4. Flat Bed, On-Off Sliding

[38] This calculation is aimed at investigating the Weertman effect [*Weertman*, 1976] at no-slip/slip boundaries. Figure 7 shows FS and SIA streamlines for flows with sliding at the beds in the middle section and a fixed bed at the edges. Where the bed is sliding, the mean slip ratio is $C_o = 10$. The bed is flat. Again, there is a strong surface response at long wavelength, but here the FS and SIA streamlines are rather different, especially toward the base of the glacier.

5.2.5. Amplitude Effects: Perturbation to Basal Topography, No Sliding

[39] By construction analyses using linearization methods assume that amplitude of response is directly proportional to forcing. In these "finite amplitude" calculations we investigate this assumption. Figure 8 shows the effect of bed topography amplitude on isochrone architecture for flow with a fixed bed. At greater amplitude the FS solution shows that overriding is more marked, both for the short wavelength case and the longer wavelength case. It seems that as the amplitude increases, the thickness of the stagnant zone increases, which explains this behavior. Similar effects for very short wavelength flows were noted by *Gudmundsson* [1997].

5.3. Numerical Perturbation Solutions for Nonlinear Rheologies

[40] Perturbation solutions for nonlinear rheologies are computed numerically using the methodology described by *Hindmarsh* [2004]. Isothermal and thermomechanically coupled cases are presented. Extensions to this theory are presented in Appendix A, which considers thermal coupling and the perturbed age equation. Isothermal results are

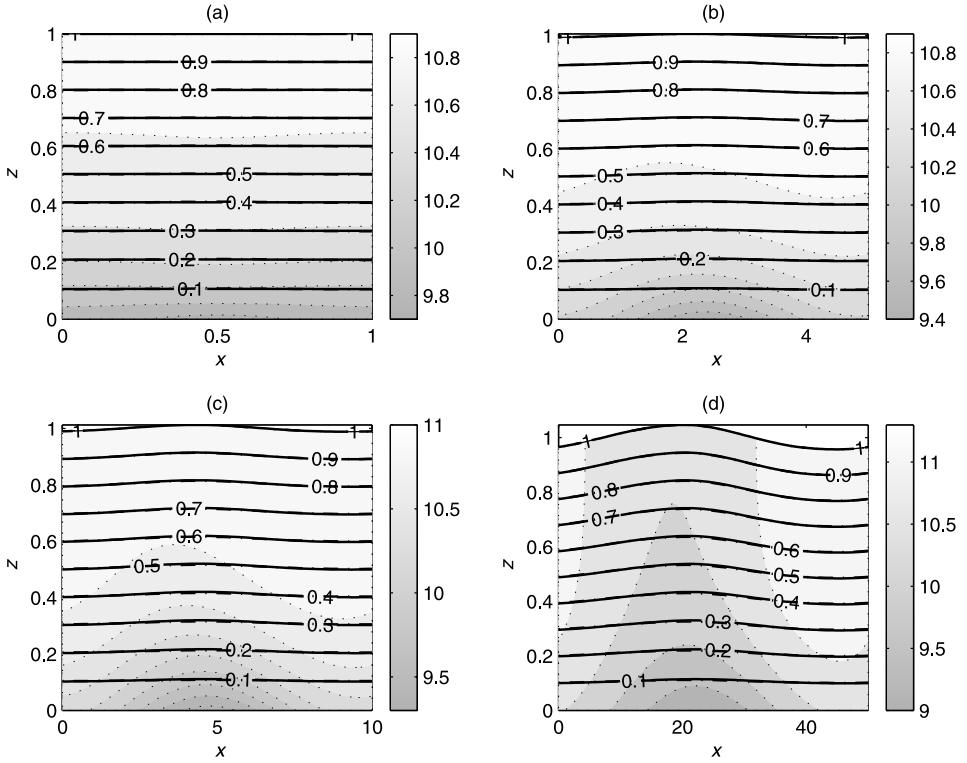

Figure 6. Calculation showing effect of sliding perturbations on full-system finite amplitude calculations of streamlines/isochrones. Ice is sliding over bed with mean slip ratio C_o of 10, but with sinusoidally varying slipperiness with amplitude 0.2. Bed is flat. See Figure 4 caption for meaning of different lines. Isochrone geometry is mainly determined by surface response, which is stronger at long wavelengths. SIA isochrones correspond to FS isochrones.

presented in a dimensionless system, with one consistent set of units roughly corresponding to an ice-mass with $\tilde{A}_c = 5 \times 10^{-24}\text{Pa}^{-3}\text{.s}$, $\tilde{a} = 0.1\text{m.a}^{-1}$, $\tilde{\rho} = 917\text{kg.m}^{-3}$, $\tilde{g} = 9.81\text{m.s}^{-2}$, $\tilde{H} = 2000\text{m}$. The parameters as specified create an upper surface velocity of roughly 5×10^2 m.a^{-1}. The Glen index $n = 3$. The thermally coupled results are presented in physical units.

[41] Also discussed are isochrones computed using the longitudinal stress approximation of *Blatter* [1995], using the perturbation method of *Hindmarsh* [2004]. The reduced set of equations used here corresponds to model LMLa in that paper.

[42] Various cases repeating the studies for fixed bed and sliding with varying bed topography were made (not shown), which gave similar results. Some computations were carried out at very high slip ratio, but the same basic pattern of overriding at short wavelengths was still maintained. Amplitude effects are an intrinsically nonlinear phenomenon which cannot be investigated by linearized techniques.

5.3.1. Relationship Between Streamlines and Isochrones

[43] First, we wish to demonstrate the validity of the analysis presented in section 4 concerned with the relationship between streamlines and isochrones. Figure 9 demonstrates the close relationship between isochrones and streamlines for FS plane flow. This correspondence underlies the applicability of the finite element streamline calculations to understanding isochrone behavior. Superimposed on the FS isochrones are markers indicating the longitudinal stress approximation. These are virtually coincident, showing that the longitudinal stress approximation gives remarkably accurate isochrones.

5.3.2. Three-Dimensional Effects

[44] Although it is not usually apparent in radargrams, bedrock topography is three-dimensional and the transverse variation is expected to affect radar line geometry. Figure 9 also shows steady isochrones for three-dimensional flows. Four different configurations are shown, indicated in the caption, with (Figure 9a) and (Figure 9c) having infinite transverse wavelengths, and (Figures 9b and 9b) unit transverse wavelengths. The shorter of the two wavelengths L_x, L_y determines whether overriding or draping occurs. Superimposed on the FS isochrones are markers indicating the longitudinal stress approximation. Again, these are virtually coincident with the FS solution.

5.3.3. Thermomechanical Coupling

[45] Finally, the question arises as to whether additional physical processes will affect the geometry of radar lines. Figure 10 shows steady isochrones for a thermomechanically coupled flow. In such flows there are four free dimensionless parameters corresponding to slope, surface temperature, geothermal heat flux and accumulation rate. Presenting the results in a dimensionless system overcomplicates matters unnecessarily for the simple demonstration required here. The base flow is 2500 m thick, with surface

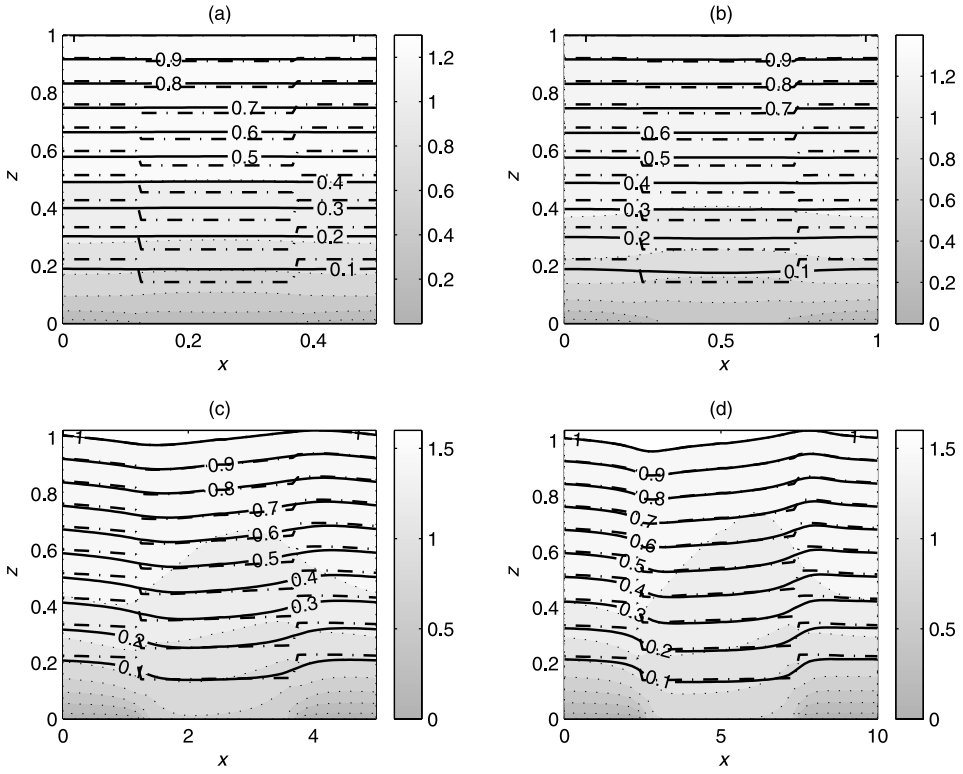

Figure 7. Calculation showing effect of sliding perturbations on full-system finite amplitude calculations of streamlines/isochrones. Ice is sliding over bed in middle and is fixed at edges. Bed is flat. See Figure 4 caption for meaning of different lines. Isochrone geometry shows Weertman effect (dipping at no-slip/slip boundary and reverse Weertman effect (rising at slip/no-slip boundary). FS shows smoother response than SIA, and effect is weak at short wavelengths.

temperature -36.125°C, slope 0.0025, accumulation rate 0.1 m yr^{-1} and geothermal heat flux 50 mW m^{-2}. In the base flow, the basal temperature was computed to be -1.6°C.

[46] Cases with wavelength 0.4 times the ice thickness and 4 times the ice thickness are shown. The usual pattern is demonstrated, with isochrones tending to override at shorter wavelengths and drape at longer wavelengths. Some intricate temperature perturbations induced by the presence of basal topography do not apparently affect the dominance of mechanical effects. As before, the longitudinal stress approximation is remarkably accurate.

5.3.4. Parameter Studies

[47] We have focused on the effects of wavelength on radar layer geometry. *Gudmundsson* [2003] shows that two further relevant parameters are slope and slip ratio. Summaries of calculations varying these two parameters are presented here.

[48] Figure 11 shows some extended parameter studies. Figure 11a is a similar diagram to 3 d, showing deflection from the SIA prediction as a function of elevation and wavelength. As wavelength gets shorter, the point of maximum deflection moves downward, but at wavelengths shorter than one ice sheet thickness, the longitudinal stress approximation becomes poor. At longer wavelengths, rather greater than the ice thickness, the LSA is excellent. The deflection pattern for sliding shows a more complex dependence on wavelength, and the point of maximum deflection is higher than in the case of no slip. However, the difference between sliding and no sliding is less than that caused by wavelength.

[49] Figure 11b shows the effect of slope and wavelength on maximum deflection. Wavelength has the dominant effect, and where slope becomes comparably important it is at longer wavelengths where the deflection is lower.

[50] Figure 11c shows the effect of slip ratio and wavelength on maximum deflection. Again, wavelength has the dominant effect, although the maximum deflection is sensitive to slip ratios where this value is around 1.

[51] Figure 11d shows, in more detail, for the case of a fixed bed, the dependence of the maximum deflection on the two orthogonal wavelengths. This figure supports the statement made above that the shorter of the wavelengths determines the deflection.

6. Conclusions and Discussion

[52] 1. Isochrones track streamlines for sufficiently short wavelengths $\tilde{L}_x \ll \tilde{H}\dfrac{\tilde{u}_x}{\tilde{a}}$ in dimensional units or $L_x < \mathcal{O}(1/a)$ in dimensionless units, where the wavelength has been scaled by the ice thickness. Since the accumulation rate a is scaled relative to the horizontal velocity, and can thus be $\ll 1$, this effect can happen over quite long wavelengths.

[53] 2. Analytical, semianalytical and numerical solutions all show same features. At short wavelengths streamlines and isochrones override basal topography, while at longer

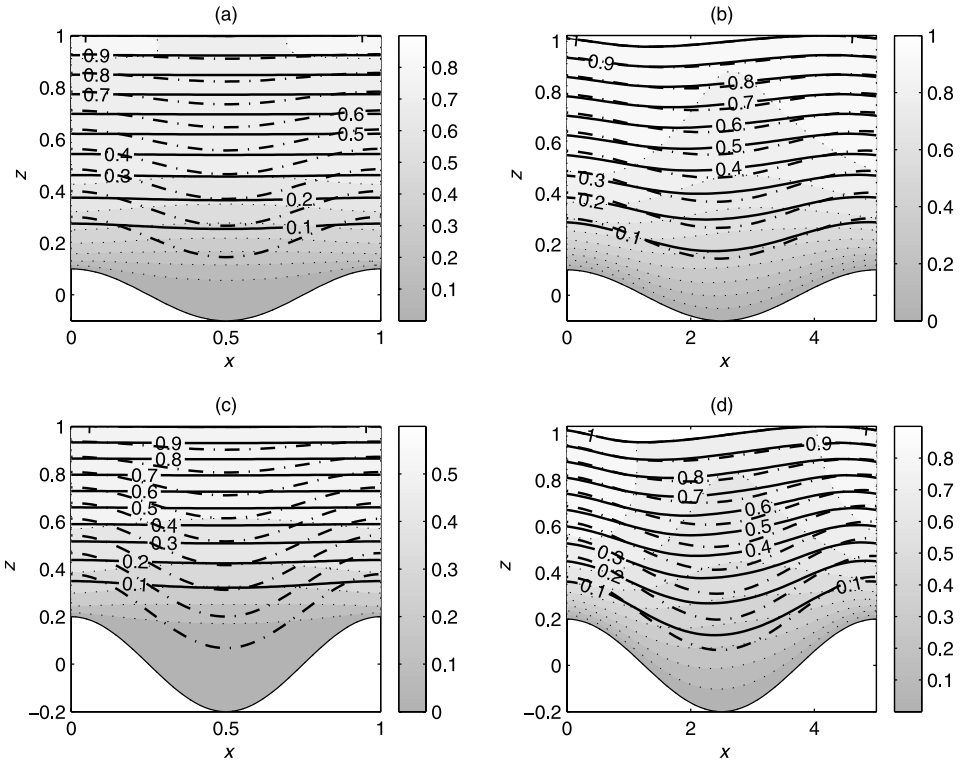

Figure 8. Calculation showing effect of bed perturbations on full system finite amplitude calculations of streamlines/isochrones, showing the effect of amplitude on isochrone geometry. Ice is fixed to bed. See Figure 4 caption for meaning of different lines. Overriding of FS isochrones occurs for short wavelengths; draping occurs at long wavelengths. Overriding is more marked for greater amplitudes. Results are compared for two different wavelengths (L = 1, 5) and two different amplitudes (0.1, 0.2). Dotted line is horizontal velocity.

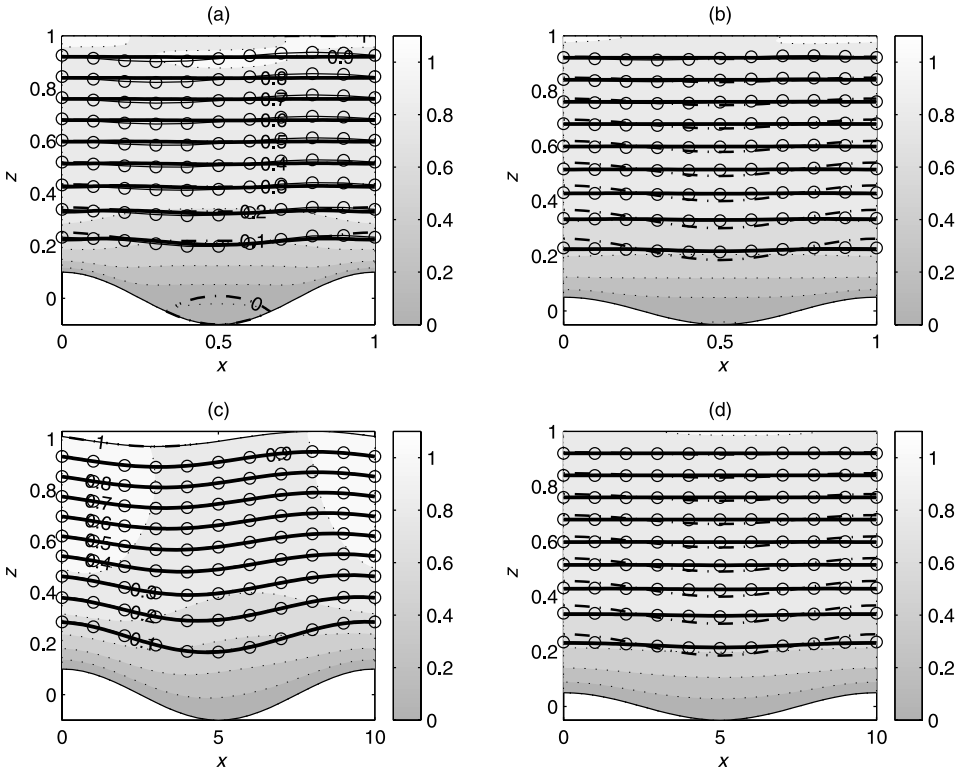

Figure 9. Computed isochrones for plane flow, using a perturbation method, full-system nonlinear rheology (solid line). Also indicated are isochrones computed using longitudinal stress approximation (circled line nearly coincident with full-system lines). Background contouring is the horizontal velocity. (a, c) Flow is plane, and the dash-dotted line is streamline. Isochrones and streamlines are coincident in Figure 9c and mostly coincident in Figure 9a. (b, d) Influence of three-dimensional bed topography on isochrone architecture using a perturbation method is shown. The horizontal wavelength is indicated, transverse wavelength is 1; amplitude of transverse perturbation is the same as that of longitudinal perturbation. Dashed lines are SIA isochrones. Comparison of Figures 9c and 9d shows that isochrone deflection is dominated by shorter of the two wavelengths, while Figures 9a and 9b show that the addition of a comparable transverse wavelength does not significantly affect architecture.

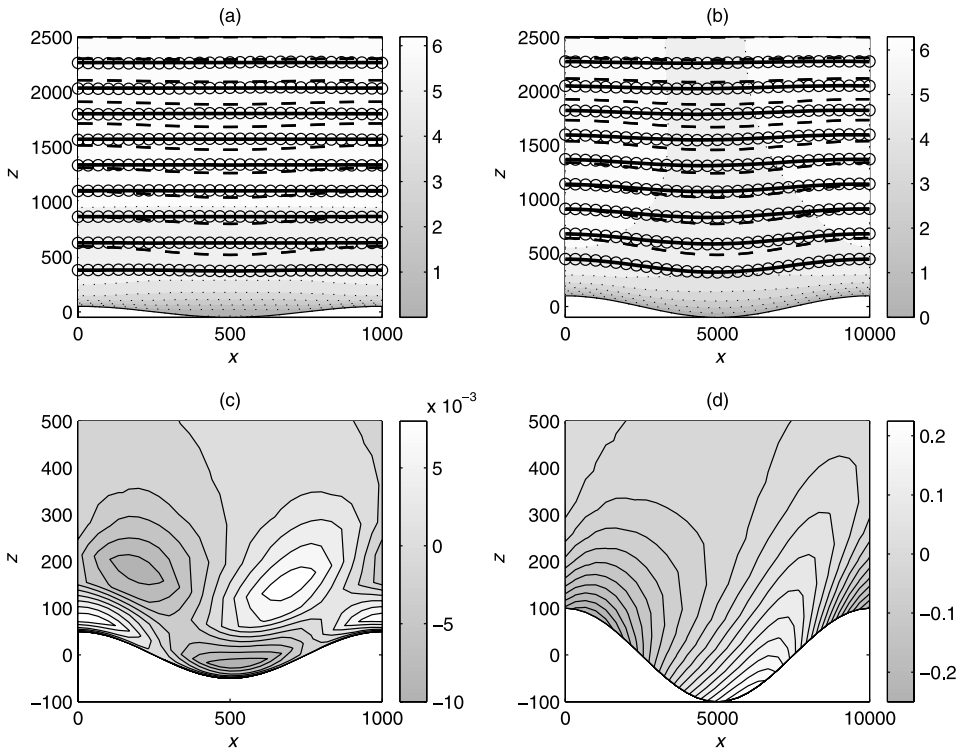

Figure 10. Influence of thermally dependent ice viscosity on isochrone architecture using a perturbation method, nonlinear rheology. (a, b) Longitudinal wavelength indicated, for indicated wavelength. Also indicated are isochrones computed using longitudinal stress approximation (dots nearly coincident with full-system lines). Dash-dotted lines are SIA streamlines. (c, d) Temperature perturbation in °C. Qualitatively, the results are as for the isothermal cases, showing that the complex thermal structure seems to be markedly less important than mechanical effects.

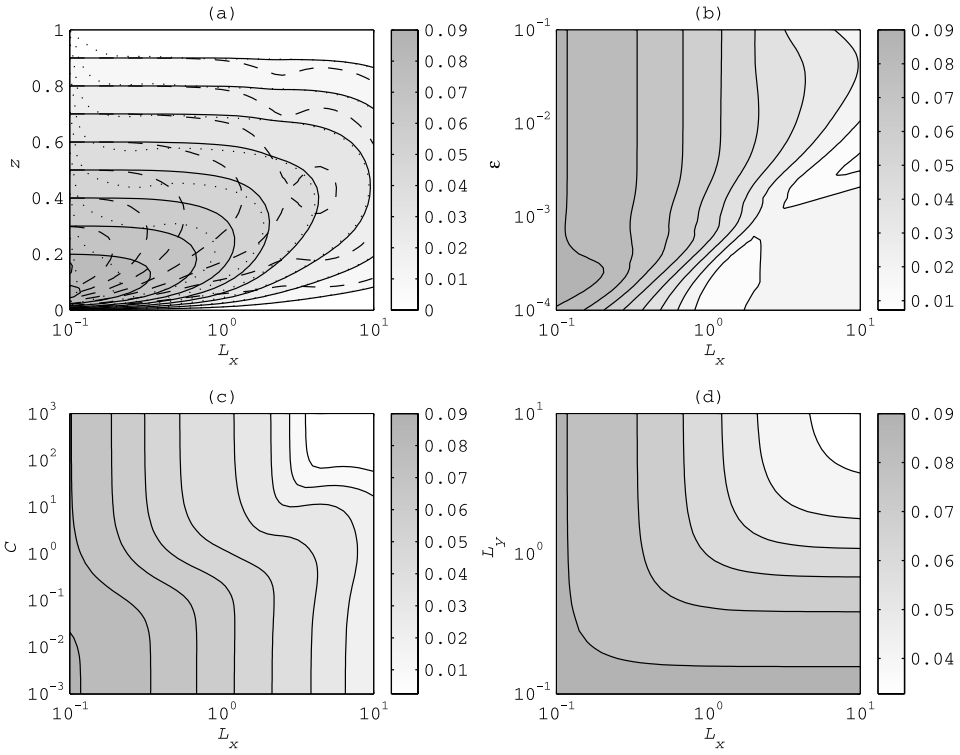

Figure 11. Studies of deviation from SIA prediction as a function of slope, slip ratio and wavelength computed using a perturbation method, full-system nonlinear rheology. (a) Isochrone deflection of the full-system isochrones from the SIA isochrones as a function of elevation and wavelength for no slip (solid line and background coloring), sliding with slip ratio 10 (dashed line), and longitudinal stress approximation, no slip (dotted line). (b) Maximum deflection as a function of longitudinal wavelength L_x and slope ε. (c) Maximum deflection as a function of L_x and slip ratio C. (e) Maximum deflection as a function of L_x and transverse wavelength h L_y.

wavelength, they track or drape the basal and surface topography.

[54] 3. Streamlines have constant normalized elevation for flows satisfying the SIA. Isochrones show the same behavior over short wavelengths.

[55] 4. The flow style, overriding or draping, is determined by the direction of the shorter of the two wavelengths characterizing any two-dimensional surface. Thus overriding can occur at long wavelengths in radar lines following the flow direction, but in such a case one should suspect the presence of short-wavelength topography orthogonal to the section.

[56] 5. Flow by sliding does not alter these conclusions.

[57] 6. Thermal coupling does not alter these conclusions.

[58] 7. Isochrones computed using the longitudinal stress approximation correspond remarkably well to the full-system solutions for the small-amplitude cases considered here. Comparison of finite amplitude LSA and FS solutions is needed to assess the general validity of this behavior.

6.1. Discussion: Overriding, Draping, and the Degree of Surface Transfer

[59] We have seen that wavelength has the strongest signal: At long wavelengths, the isochrones drape, while at short wavelengths they override. It is known that the transfer of the basal signal to the surface is wavelength dependent [*Gudmundsson*, 2003], with strong transfer at long wavelength, and extremely limited transfer at short wavelengths. It is likely that the weak transfer at short wavelengths and the observations of isochrone overriding are essentially the same phenomenon.

[60] *Gudmundsson* [2003] also points out that transfer is much stronger when the slip ratio is high for intermediate wavelengths (5 to 10 ice thicknesses). By the argument presented above, this would imply that the deflection from the SIA isochrones would be smaller when sliding is occurring at these wavelengths. This proposition is consistent with Figures 11a and 11c as well Figures 4c and 5c.

6.2. Discussion: Is There a Traction Signal?

[61] Given that glacier mechanics is dominated by two parameters, wavelength/aspect ratio and slip ratio/traction number [e.g.,*Gudmundsson*, 2003], it is somewhat surprising that the wavelength signal is so much more obvious than the traction signal.

[62] There are hints that the slip ratio affects the deviation of FS solutions from SIA solutions. Comparison of Figures 4a and 5a shows that at short wavelength the mean difference between FS and SIA is greater when sliding is occurring, though the degree of overriding (measured by the flatness of the streamline) is greater for no slip.

[63] Taking into account this observation as well as the results shown in Figure 11c, one can say that there is a weak traction/slip ratio signal in layer architecture. The use of this

to invert for the slip ratio from radar lines, where one of the wavelength components is unknown, would appear to be rather difficult.

6.3. Discussion: Why is the LSA So Good?

[64] A second surprise is how good the LSA is. Theory suggests that it is valid down to wavelengths with dimension equal to a few ice sheet thicknesses, but the calculations in this paper show that this is a conservative error estimate, and that the LSA gives good approximations down to wavelengths of one ice thickness.

[65] Apparently, the LSA manages to capture the stagnation in hollows, which allows the LSA to be able to represent overriding. This in turn means that LSA predictions are good in the upper part of the ice, at least for steady state. One should not expect the LSA to be good near the base of the ice sheet at short wavelength, but it is here where quite often radar layer observations cannot be made.

Appendix A: Linearization of the Governing Equations

A1. Momentum Balance

[66] The linearized stress equations are given by equations (A1) to (A9) in the work by *Hindmarsh* [2004] with the exception that the first-order viscosity given by *Hindmarsh's* [2004] equation (A6) is now given by

$$\hat{\eta}^{(1)} = \frac{1-n}{n}\frac{\eta^{(0)}}{e^{(0)2}}\left(e_{xz}^{(0)}\hat{e}_{xz}^{(1)} + \frac{1}{2}e_{xx}^{(0)}\left(\hat{e}_{xx}^{(1)} - \hat{e}_{zz}^{(1)}\right)\right) + \eta^{(0)}\frac{B'\left(\theta^{(0)}\right)}{B\left(\theta^{(0)}\right)}, \tag{A1}$$

where the difference between the isothermal and present treatments is the second term on the right-hand side.

A2. Age Equation

[67] In scaled form, the steady age equation (11) is given by

$$\frac{\zeta\nabla\cdot Q - \nabla\cdot\boldsymbol{q} - \zeta(a-m) - m}{H}\partial_\zeta X + \boldsymbol{u}\cdot\nabla_{\mathrm{H}}X = 1, \tag{A2}$$

where

$$\mathrm{q} = \int_0^\zeta \mathrm{ud}\zeta', \mathrm{Q} = \int_0^1 \mathrm{ud}\zeta', \tag{A3}$$

This can be readily seen from equation (37) of *Hindmarsh*, [1999]. In steady state, one can use

$$\nabla\cdot Q \equiv (a-m)$$

to write this as

$$\boldsymbol{u}\cdot\nabla_{\mathrm{H}}X - \frac{\nabla\cdot\boldsymbol{q}+m}{H}\partial_\zeta X = 1. \tag{A4}$$

[68] Linearization of the age equation (A4) gives at zeroth order

$$\frac{\left(a^{(0)}-m^{(0)}\right)\boldsymbol{\omega}^{(0)}(\zeta)+m^{(0)}}{H^{(\mathbf{0})}}\frac{\partial X^{(0)}}{\partial\zeta} = 1, \tag{A5}$$

$$\omega^{(0)}(\zeta) = q_x^{(0)}/Q_x^{(0)}, \tag{A6}$$

and at first order the steady perturbation equation is

$$\boldsymbol{u}^{(0)}\cdot\nabla_H X^{(1)} - \frac{\nabla\cdot\boldsymbol{q}^{(0)}+m}{H^{(0)}}\frac{\partial X^{(1)}}{\partial\zeta} + \boldsymbol{u}^{(1)}\cdot\nabla_H X^{(0)} + \frac{\nabla\cdot\boldsymbol{q}^{(0)}+m}{H^{(0)2}}\frac{\partial X^{(0)}}{\partial\zeta}H^{(\mathbf{1})} - \frac{\nabla\cdot\boldsymbol{q}^{(\mathbf{1})}}{H^{(0)}}\frac{\partial X^{(0)}}{\partial\zeta} = 0, \tag{A7}$$

which simplifies to

$$\mathrm{i}k_x u_x^{(0)}\hat{X}^{(1)} + \frac{\nabla\cdot\boldsymbol{q}^{(0)}+m}{H^{(0)}}\frac{\partial\hat{X}^{(1)}}{\partial\zeta} = \mathrm{i}\frac{\left(k_x q_x^{(1)} + k_y q_y^{(1)}\right)}{H^{(0)}}\cdot\frac{\partial X^{(0)}}{\partial\zeta} + \frac{\nabla\cdot\boldsymbol{q}^{(0)}+m}{H^{(0)2}}\frac{\partial X^{(0)}}{\partial\zeta}\hat{H}^{(\mathbf{1})}, \tag{A8}$$

and since we can also write

$$\nabla\cdot\boldsymbol{q}^{(0)} = (a-m)\boldsymbol{\omega}^{(0)}(\zeta),$$

the first-order steady age equation can also be written as

$$\mathrm{i}k_x u_x^{(0)}\hat{X}^{(1)} + \frac{\left(a^{(0)}-m^{(0)}\right)\boldsymbol{\omega}^{(0)}(\zeta)+m^{(0)}}{H^{(0)}}\frac{\partial\hat{X}^{(1)}}{\partial\zeta} = \mathrm{i}\frac{\boldsymbol{k}\cdot\hat{\boldsymbol{q}}^{(1)}}{H^{(0)}}\frac{\partial X^{(0)}}{\partial\zeta} + \frac{\hat{H}^{(\mathbf{1})}}{H^{(0)}}, \tag{A9}$$

where the zeroth-order solution has been used to simplify the last term on the right-hand side.

[69] The deviation of an isochrone with normalized elevation $\zeta_i(x)$ is given by

$$\partial_\zeta X^{(0)}\hat{\zeta}_i^{(1)} = -\hat{X}^{(1)}. \tag{A10}$$

With zero accumulation and melting, the Fourier-transformed ageing equation (A8) becomes

$$\mathrm{i}k_x u_x^{(0)}\hat{X}^{(1)} = \mathrm{i}\frac{\left(k_x\hat{q}_x^{(1)} + k_y\hat{q}_y^{(1)}\right)}{H^{(0)}}\frac{\partial X^{(0)}}{\partial\zeta} + \frac{\hat{H}^{(1)}}{H^{(0)}}, \tag{A11}$$

yielding this solution for the first-order age perturbation,

$$\hat{X}^{(1)} = \frac{\left(\hat{q}_x^{(1)} + \frac{k_y}{k_x}\hat{q}_y^{(1)}\right)}{u_x^{(0)}H^{(0)}}\frac{\partial X^{(0)}}{\partial\zeta} - \frac{\mathrm{i}\hat{H}^{(1)}}{k_x u_x^{(0)}H^{(0)}}, \tag{A12}$$

and use of equation (A10) gives the isochrone deflection as

$$\hat{\zeta}_1 = -\frac{\left(\hat{q}_x^{(1)} + \frac{k_y}{k_x}\hat{q}_y^{(1)}\right)}{u_x^{(0)}H^{(0)}} + \frac{\mathrm{i}\hat{H}^{(1)}}{k_x u_x^{(0)}\frac{\partial X^{(0)}}{\partial\zeta}H^{(0)}}. \tag{A13}$$

Since $\frac{\partial X_{(0)}}{\partial\zeta} = \mathcal{O}(1/a)$, the last equation can be written

$$\hat{\zeta}_1 = -\frac{\left(\hat{q}_x^{(1)} + \frac{k_y}{k_x}\hat{q}_y^{(1)}\right)}{u_x^{(0)}H^{(0)}} + \mathcal{O}(aL_x), \tag{A14}$$

and the previous results about isochrones tracking streamlines are immediately obtained. The flux gradient can be

related to terms in the *Gudmundsson* [2003] full-system solution and the *Hindmarsh* [2004] longitudinal stress correction solution by the expression

$$-\mathrm{i}k_x\hat{q}_x^{(1)} = -\hat{w}^{(1)} - \mathrm{i}k_x(\zeta\hat{H}^{(1)} + \hat{b}^{(1)}).$$

A3. Heat Equation

[70] In scaled form, the heat equation (7) is

$$\partial_t\theta + \boldsymbol{u}\cdot\boldsymbol{\nabla}\theta + \frac{\zeta\boldsymbol{\nabla}\cdot\boldsymbol{Q} - \boldsymbol{\nabla}\cdot\boldsymbol{q} - (a-m)\zeta - m}{H}\partial_\zeta\theta = \frac{\beta}{H^2}\partial_\zeta^2\theta + \beta\left(\partial_x + \frac{\partial_x\tilde{Z}}{H}\partial_\zeta\right)^2\theta + \beta\left(\partial_y + \frac{\partial_y\tilde{Z}}{H}\partial_\zeta\right)^2\theta + \chi\boldsymbol{\tau}\cdot e, \tag{A15}$$

which is equivalent to that given by *Hindmarsh* [1999, equation (36)], apart from the horizontal conduction terms (second and third terms on right-hand side), which follow simply from the differential transforms for the normalized coordinate. The parameters are given by

$$\beta = \frac{\kappa}{\tilde{H}_*\tilde{v}_*}, \chi = \frac{\varepsilon\tilde{\rho}\tilde{g}\tilde{H}_*}{\tilde{\rho}\tilde{c}}. \tag{A16}$$

Linearization and Fourier transformation of the scaled heat equation leads to

$$\begin{aligned}\lambda\hat{\theta}^{(1)} = {} & \mathrm{i}k_x u_x^{(0)}\hat{\theta}^{(1)} + \frac{\omega^{(0)}(a-m)+m}{H^{(0)}}\partial_\zeta\hat{\theta}^{(1)} + \\ & \frac{\beta}{H^{(0)2}}\partial_\zeta^2\hat{\theta}^{(1)} - \beta|\boldsymbol{k}|^2\hat{\theta}^{(1)} + \beta|\boldsymbol{k}|^2\frac{\partial_\zeta\theta^{(0)}}{H^{(0)}}\tilde{b}^{(1)} - \\ & \left(\frac{\omega^{(0)}(a-m)+m-\zeta|\boldsymbol{k}|^2\beta}{H^{(0)2}}\partial_\zeta\theta^{(0)} + 2\frac{\beta}{H^{(0)3}}\partial_\zeta^2\theta^{(0)}\right)\hat{H}^{(1)} \\ & + \mathrm{i}\frac{\zeta\boldsymbol{k}\cdot\hat{\mathbf{Q}}^{(1)} - \boldsymbol{k}\cdot\hat{\mathbf{q}}^{(1)}}{H^{(0)}}\partial_\zeta\theta^{(0)} + \chi\boldsymbol{\tau}^{(0)}\cdot\tilde{\boldsymbol{e}}^{(1)} + \chi\tilde{\boldsymbol{\tau}}^{(1)}\cdot\mathbf{e}^{(0)},\end{aligned} \tag{A17}$$

with

$$\boldsymbol{\tau}^{(0)}\cdot\hat{\boldsymbol{e}}^{(1)} = 2\tau_{xz}^{(0)}\hat{e}_{xz}^{(1)} + \tau_{xx}^{(0)}\left(\hat{e}_{xx}^{(1)} - \hat{e}_{zz}^{(1)}\right) \tag{A18}$$

$$\hat{\boldsymbol{\tau}}^{(1)}\cdot\boldsymbol{e}^{(0)} = 2e_{xz}^{(0)}\hat{\tau}_{xz}^{(1)} + e_{xx}^{(0)}\left(\hat{\tau}_{xx}^{(1)} - \hat{\tau}_{zz}^{(1)}\right). \tag{A19}$$

Appendix B: Implementation of Sliding in the Finite Element Calculations

[71] A commercial finite element (FE) program (MARC) has been used to calculate the steady state geometry and its flow field of an inclined ice mass flowing over a perturbed bed. The program solves the full Stokes equations. The flow field of this full-system (FS) model is then compared with the flow field obtained from the shallow ice approximation (SIA) model for the steady state geometry and the boundary conditions as obtained and used in the FS model. For a full description of the calculations the reader is referred to *Raymond and Gudmundsson* [2005].

[72] In this appendix all quantities are taken to be dimensional. The model geometry comprises a 2-D plane flow model, inclined at 3°. Steady state surface geometry was computed by evolving the surface geometry to a steady state. The numerical calculations never suggested that there was more than one steady configuration. Four different sets of experiments with varying amplitudes (0.1, 0.2) and wavelengths were computed for the following configurations: (1) undulating bed, comprising (set a) ice frozen to bed and (set b) ice mass sliding over bed with a constant sliding factor ($C_o = 10$), and (2) flat bed, comprising (set c) sinusoidal perturbation in slipperiness and (set d) step change in sliding behavior (no sliding-sliding-no sliding).

[73] These results are compared with the flow field for the SIA model. This is not exactly the SIA model, as the surface geometry used is the one computed using the FS velocity field. However, the transfers of bed to surface for FS and SIA are rather similar [*Gudmundsson*, 2003; *Raymond and Gudmundsson*, 2005], so this does not significantly distort the results. The fluxes of the two models are compared by using a flux normalized with the FS surface flux. In steady state this is constant for plane flow. Therefore the normalized flux for the SIA model is obtained by integrating the velocity shape function over depth and for the FS model by integrating the FS velocity over depth and dividing it by its surface flux.

[74] To account for sliding at the glacier base, a relation between sliding velocity v_b and basal shear traction τ_b is assumed,

$$u_{x(b)} = C(x)\tau_{xz(b)}^{n'}, \tag{B1}$$

where $C(x)$ is the slip ratio and n' a parameter to be specified *Lliboutry*, 1968, 1979]. This relation for sliding is implemented in the numerical model by adding a thin soft layer at the glacier base [*Schweizer and Iken*, 1992; *Vieli et al.*, 2000] with a flow law corresponding to equation (5) and with flow parameters n' and A'. Since the layer is thin, we can assume that within this layer, the shallow ice approximation holds.

$$\mathsf{e} = A'|\tau|^{n'-1}\boldsymbol{\tau}.$$

[75] In the FS model the rate factor A or A' is used as an input parameter. For the basal layer an $A'(x)$ is calculated to correspond to the slip ratio $C(x)$. From equation (B1) we know that the $C(x)$ is proportional to v_b. For an ice slab with thickness h, with an underlying thin soft layer of thickness d and slope angle ε the analytical solution of the basal velocity v_b at the ice interface in the shallow ice approximation [*Hutter*, 1983] is

$$u_{x(b)} = \int_0^d 2A'\tau_{xz}^{n'}dz, \tag{B2}$$

where the basal shear traction is given by

$$\tau_{xz} = \rho g(h+d-z)\sin\varepsilon. \tag{B3}$$

The basal velocity of the ice is then given by computing the integral of equation (B2),

$$\begin{aligned}u_{x(b)} &= \int_0^d 2A'(\rho g\sin\varepsilon)^{n'}(h+d-z)^{n'}dz \\ &= \frac{2A'}{n'+1}(\rho g\sin\varepsilon)^{n'}\left((h+d)^{(n'+1)} - h^{(n'+1)}\right),\end{aligned}$$

and using (B1) to obtain $C(x)$. For the case of the thin soft basal layer the flow exponent is chosen to be $n' = 1$.

[76] In the model experiments the mean slip ratio C_o is given and used to calculate the rate factor A'. A sliding constant A''_o is defined by

$$A''_o = C_o \frac{n'+1}{2} \frac{1}{(h_o+d)^{(n'+1)} - h_o^{(n'+1)}}. \tag{B4}$$

This value of A''_o is used in the constant sliding experiments (section 5.2.2). It is also used in the definition of the sinusoidally varying sliding (section 5.2.3),

$$A'(x) = A''_o(1 + \gamma \cos(k_x x)), \tag{B5}$$

where γ is the amplitude of the perturbation. It is also used in the on-off sliding

$$A'(x) = A''_o \qquad 0 \le x < L/3, 2L/3 \le x < L \tag{B6}$$

$$A'(x) = 0 \qquad L/3 \le x < 2L/3. \tag{B7}$$

For the cases of constant slipperiness and sinusoidally varying slipperiness, the mean slip ratio $C_0 = 10$, while for the cases of on/off sliding, the slip ratio alternated between 0 and 1.

[77] The computational grid comprised (61 × 31) nodes (fixed bed) (section 5.2.1). For the sliding cases extra nodes were used to represent the thin deforming layer, which was 2/30th the thickness of the ice sheet for constant sliding with a (61 × 33) grid (§5.2.2), and for the spatially variable sliding a (61 × 32) grid with a layer thickness of 1/30 (sections 5.2.3 and 5.2.4).

Appendix C: SIA Shape Functions

[78] As described by *Paterson* [1994, p. 251], where flow is by internal deformation only, the velocity at depth $H(1\text{-}\zeta)$, can be written in terms of the mean velocity as

$$u_x(x,\zeta) = \bar{u}\frac{n+2}{n+1}\left(1 - (1-\zeta)^{n+1}\right) \tag{C1}$$

$$= \bar{u}(x)\upsilon^{(D)}(\zeta), \tag{C2}$$

where

$$\upsilon^{(\mathrm{D})}(\zeta) = \frac{n+2}{n+1}\left(1 - (1-\zeta)^{n+1}\right) \tag{C3}$$

is the shape function of the horizontal velocity with depth and is the mean velocity.

[79] The flux of the SIA model can be calculated by multiplying the surface flux from the FS model with the shape function of the flux with depth $\omega^{(\mathrm{D})}(\zeta)$

$$\omega^{(\mathrm{D})}(\zeta) = \int_0^\zeta \upsilon^{(D)}(\zeta) d\zeta' \tag{C4}$$

$$= \frac{(n+2)\zeta + (1-\zeta)^{n+2} - 1}{n+1}. \tag{C5}$$

For pure basal sliding,

$$\upsilon^{(\mathrm{S})}(\zeta) = 1, \omega^{(\mathrm{S})}(\zeta) = \zeta, \tag{C6}$$

while for combinations of internal deformation and basal sliding,

$$\upsilon(\zeta) = \frac{1}{1+C}\upsilon^{(\mathrm{D})}(\zeta) + \frac{C}{1+C}\upsilon^{(S)}(\zeta) \tag{C7}$$

$$\omega(\zeta) = \frac{1}{1+C}\omega^{(\mathrm{D})}(\zeta) + \frac{C}{1+C}\omega^{(\mathrm{S})}(\zeta). \tag{C8}$$

[80] **Acknowledgment.** This work was supported by NERC grant NER/A/S/2001/01011 "Calculation of ice accumulation rates in Antarctica over the last glacial cycle."

References

Blatter, H. (1995), Velocity and stress-fields in grounded glaciers: A simple algorithm for including deviatoric stress gradients, *J Glaciol.*, *41*(138), 333–344.

Gudmundsson, G. H. (1997), Basal flow characteristics of a non-linear flow sliding frictionless over strongly undulating bedrock, *J. Glaciol.*, *42*(143), 80–89.

Gudmundsson, G. H. (2003), Transmission of basal variability to a glacier surface, *J. Geophys. Res.*, *108*(B5), 2253, doi:10.1029/2002JB002107.

Hempel, L., F. Thyssen, N. Gundestrup, H. B. Clausen, and H. Miller (2000), A comparison of radio-echo sounding data and electrical conductivity of the GRIP ice core, *J. Glaciol.*, *46*(154), 369–374.

Hindmarsh, R. C. A. (1999), On the numerical computation of temperature in an ice-sheet, *J. Glaciol.*, *45*(151), 568–574.

Hindmarsh, R. C. A. (2004), A numerical comparison of approximations to the Stokes equations used in ice-sheet and glacier modeling, *J. Geophys. Res.*, *109*, F01012, doi:10.1029/2003JF000065.

Hindmarsh, R. C. A., and K. Hutter (1988), Numerical fixed domain mapping solution of free surface flows coupled with an evolving interior field, *Int. J. Numer. Anal. Methods Geomech.*, *12*, 437–459.

Hutter, K. (1983), *Theoretical Glaciology*, D. Riedel, Norwell, Mass.

Leysinger Vieli, G. J.-M. C., and G.H. Gudmundsson (2004), On estimating length fluctuations of glaciers, *J. Geophys. Res.*, *109*, F01007, doi:10.1029/2003JF000027.

Lliboutry, L. A. (1968), General theory of subglacial cavitation and sliding of temperate glaciers, *J. Glaciol.*, *7*(49), 21–58.

Lliboutry, L. A. (1979), Local friction laws for glaciers: A critical review and new openings, *J. Glaciol.*, *23*(89), 67–95.

Paterson, W. S. B. (1994), *Physics of Glaciers*, third ed., Elsevier, New York.

Pattyn, F. (2002), Ice-flow characteristics over a rough bedrock: Implications for ice-core interpretation, *Polar Meteorol. Glaciol.*, *16*, 42–52.

Raymond, M. J., and G. H. Gudmundsson (2005), On the relationship between surface and basal properties on glaciers, ice sheets, and ice streams, *J. Geophys. Res.*, *110*, B08411, doi:10.1029/2005JB003681.

Reeh, N., and W. Paterson (1988), Application of a flow model to the ice-divide region of Devon Island ice cap, Canada, *J. Glaciol.*, *34*(116), 55–63.

Schweizer, J., and A. Iken (1992), The role of bed separation and friction in sliding over an undeformable bed, *J. Glaciol.*, *38*(128), 77–92.

Vieli, A., M. Funk, and H. Blatter (2000), Tidewater glaciers: Frontal flow acceleration and basal sliding, *Ann. Glaciol.*, *31*, 217–221.

Weertman, J. (1976), Sliding–no sliding zone effect and age determination of ice cores, *Quat. Res.*, *6*, 203–207.

G. H. Gudmundsson and R. C. A. Hindmarsh, British Antarctic Survey, High Cross, Madingley Road, Cambridge CB3 0ET, UK. (ghg@bas.ac.uk; rcah@bas.ac.uk))

G. J.-M. C. Leysinger Vieli, Bristol Glaciology Center, School of Geographical Sciences, University of Bristol, Bristol BS8 1SS, UK. (g.leysinger-vieli@bristol.ac.uk)

M. J. Raymond, Laboratory of Hydraulics, Hydrology and Glaciology, Eidgenossische Technische Hochschule (VAW ETH), CH-8092, Zurich, Switzerland. (melanie.raymond@ethz.ch)